Construction and Building Materials 323 (2022) 126587

Contents lists available at ScienceDirect

Construction and Building Materials

journal homepage: www.elsevier.com/locate/conbuildmat

Investigation on the utilization of coal gasification slag in Portland cement: Reaction kinetics and microstructure

Bo Fu [a,b], Zhenyun Cheng [a], Dezhi Wang [c], Ning Li [d,*]

[a] Collage of Civil Engineering, North Minzu University, Yinchuan 750021, China
[b] Coal Chemical Industry Technology Research Institute, Ningxia Coal Industry Co. Ltd, National Energy Group, Yinchuan 720021, China
[c] College of Civil & Water Conservancy Engineering, Ningxia University, Yinchuan 750021, China
[d] School of Engineering, University of Glasgow, G12 8LT Glasgow, United Kingdom

ARTICLE INFO

Keywords:
Portland cement
Coal gasification slag
Reaction kinetics
Compressive strength
Microstructure

ABSTRACT

Gasification slag is a solid waste generated by the coal chemical industry which has emerged in recent years. In this paper, the effect of coal gasification slag (CGS) powder content on the reaction kinetics, gel structure and the compressive strength of Portland cement was investigated for the potential application of CGS powders in cementitious materials. The reaction and gel structure of Portland cement blended with CGS was analyzed by using X-ray diffraction, Fourier transform infrared spectroscopy and scanning electron microscopy tests. The results show that the unreacted CGS power exists mainly in an agglomerated state in cement matrix, and a low dosage of CGS powder (10%) can play a role in nucleation and pozzolanic effect in Portland cement, which is conducive to the formation of hydration reactions of Portland cement, shortening the setting time and improving the compressive strength. If the CGS content is >30%, the hydration product content decreases, and the microstructure of the sample becomes loosened. The setting times are significantly prolonged with the increase of CGS content dosing and the compressive strength is considerably reduced as well.

1. Introduction

The developments of industrialization and urbanization around the world have made Portland cement (PC) become one of the greatest industrial products on the earth, which has been inevitably and widely used in the construction of roads, bridges, buildings and other infrastructures. In the past 7 decades, the PC production amount increased nearly 35-fold [1]. However, this substantial market demand for PC has resulted in an increasingly growing consumption of natural resources and greenhouse gas emissions [2]. Therefore, the consensus on driving the development of eco-efficient PC-based material application has been mustered by research and industry communities [3-5].

Generally, there are three dominated methods of achieving the improvement of the sustainability of PC and its corresponding mortar and concrete from production to application: (i) utilization of alternative fuels to increase the energy efficiency during the production process of clinker [6], (ii) employment of solid wastes as the alternative to natural sources for the synthesis of clinkers [7], and (iii) partial replacement of PC with supplementary cementitious materials (SCMs) [8], respectively. However, the former two are less dominant compared with the use of SCMs in PC. This is because that the replacement of PC with SCMs could decrease the PC dosage in practice without scarifying the material performance [2].

There have been many types of solid wastes being widely used in PC, which contribute to avoiding the direct disposal of solid wastes such as stacking and landfill. GGBFS, steel slag and ladle slag generated from smelting process of steel as reactive mineral additive have been utilized in PC [9-11]. In addition, fly ash produced by coal combustion has been an important component in PC and concrete [12-14]. However, compared with the extensive literature on the above solid wastes, the research focused on using coal gasification slag (CGS) in PC is relatively limited. Meanwhile, in China, due to the large gasification of coal, there are about 30 million tons of CGS generated annually [15,16]. Therefore, it is of great significance to conduct research on the high-value utilization of CGS.

CGS is a by-product of the combustion and gasification of coal, which can be classified into coarse and fine slag. The particle size of fine slag is usually under 1000 μm [15]. In the coal gasification process with high temperature and pressure condition, coal particles are melted, cooled and condensed, and finally are discharged by the lock bucked at the

* Corresponding author.
E-mail address: Ning.Li@glasgow.ac.uk (N. Li).

https://doi.org/10.1016/j.conbuildmat.2022.126587
Received 1 October 2021; Received in revised form 2 January 2022; Accepted 21 January 2022
Available online 31 January 2022
0950-0618/© 2022 The Authors. Published by Elsevier Ltd. This is an open access article under the CC BY license (http://creativecommons.org/licenses/by/4.0/).

bottom of the gasifier; the slag acquired is termed as coarse CGS; on the other hand, fine CGS was obtained after collecting at the top of the gasifier, purification and precipitation by preliminary washing. However, due to the incomplete gasification, Both CGSs have a certain amount of residue carbon and are required to be further ground according to the specific uses [16]. It was reported that the mineral phases of CGSs acquired after the coal gasification contain amorphous aluminosilicate and crystal phases such as quartz, calcite, mullite and other minerals [17]. Usually, coarse CGS has a low carbon content and a potential of being mineral additive for PC, while fine CGS with a high carbon content could be used as an adsorbent or recycled alternative fuel [15]. Therefore, based on the characteristics of the above two CGSs, the attempt of using them in PC-based materials has been carried out. Yoshitaka [18] found that the concrete with fine CGS aggregate had higher compressive strength and higher drying shrinkage than that with natural aggregate. Aineto et al. [19] successfully used CGS to produce lightweight aggregate. Li et al. [15] reported that the amorphous phases from CGS powders contributed to the pozzolanic reaction with PC, while it would be impacted by residual carbon. Pomykala [20] added CGS powders into PC-based concrete and found that the inclusion of CGS powders has less influence on the compressive and flexural strengths of the concrete. However, to the best knowledge of the authors, there is no literature reported on pozzolanic activity test and reaction kinetic mechanism on the CGS with PC although a series of research have confirmed the feasibility of utilizing coarse and fine CGS in PC. It is believed that conducting study on the influence of CGS content on the pozzolanic activity test and the reaction kinetic of PC-based materials could contribute to deepening the understanding of CGS as a promising component in PC-based materials.

Moreover, the replacement of PC by adding CGS powders obtained after grinding, leads to the reduction of PC dosage, showing potentials of improving the eco-efficiency of the materials [2]. The amorphous phases in CGS can react with PC due to the pozzolanic reaction [15]. Consequently, this indicates that CGS could be potentially employed as a sustainable reactive mineral additive for PC-based materials. The purpose of this research was to systematically explore the feasibility of utilizing CGS powder as a reactive mineral additive in PC. The influences of CGS powder on the setting times, reaction kinetics, compressive strength and microstructure of the reaction products were investigated.

2. Experimental programs

2.1. Raw materials

Class P·II 52.5 PC with a specific surface area of 370 m^2/kg and a density of 3210 kg/m^3 was used in the current study. Coarse CGS collected from Ningxia Coal Group Co., Ltd., CHN Energy Group, was selected. Prior to conducting this study, coarse CGS was first dried at electric heating air-blowing drier with an electrical power of 2000 W (DHG-9243A) with a constant temperature of 60℃ for 24 h. Then, the dried CGS was ground for 60 min by using a planetary ball mill. Eventually, the CGS powder with a specific surface area of 445 m^2/kg and a density of 2550 kg/m^3 was obtained. The particle size distribution of PC and CGS powders used in this study is shown in Fig. 1. Chemical compositions of used PC and CGS powder determined by X-ray fluorescence spectroscopy (XRF) are presented in Table 1. The X-ray diffraction (XRD) patterns of PC and CGS powder used in this study are shown in Fig. 2, which shows that CGS has a certain amorphous phase at between 20 and 35°, assigned to amorphous aluminosilicate. In addition, deionized water was used to prepare the samples.

2.2. Mixture proportions and specimen preparation

In this study, a constant water-to-binder mass ratio of 0.4 was adopted. Four CSG mass ratios (10%, 30%, 50% and 70%) were adopted and 100% PC content group was prepared as the control system. The mix proportions of the specimens with different CGS powder contents are presented in Table 2.

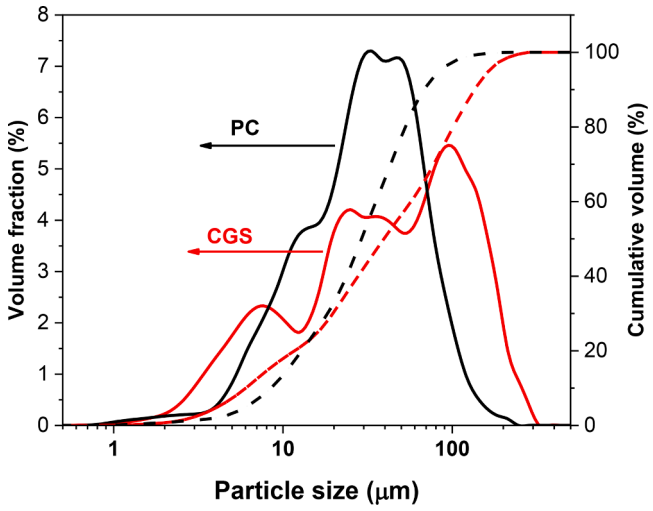

Fig. 1. Particle size distribution of PC and CGS powder.

The preparation process of all paste samples was in accordance with ASTM C305 [21]. 10 g of the fresh paste was immediately inserted in the ampoules for the isothermal calorimeter measurement when the mixing was finished. The remaining paste was cast into the molds and vibrated with a vibration table for subsequence analysis. After that, all samples within the molds were first pre-cured for 24 h at a standard curing chamber with a constant temperature of 20 ± 1℃ and relative humidity of 100%. Then, all samples were demolded and cured at the standard curing chamber with the same curing condition until testing.

2.3. Test methods

Frattini test was applied to determine the pozzolanic activity according to EN196 [22] at 2, 7 and 28 days. The pozzolanic activity of CGS was obtained by measuring its reaction with the $Ca(OH)_2$ released during the PC hydration. When the point is located below the solubility isotherm of calcium hydroxide at 40 °C, the material is considered to be pozzolanic active.

The flowability of the fresh paste was performed based on ASTM C230 [23]. The measurement of the initial and final setting time on the fresh paste was carried out by using Vicat needle apparatus based on GB/T 1346-2011 [24] (similar to ASTM C191-08 [25]) without achieving normal consistency. The influence of CGS on the reaction kinetics was investigated by using an isothermal calorimeter under a constant temperature of 20℃. The normalization of the heat flow curves was by gram of paste.

The measurement of the compressive strengths of the cubic samples with a size of 40 × 40 × 40 mm cured at 1, 7 and 28 d was conducted. The loading rate was 2.4 kN/s and the average values of the six samples were reported.

XRD and Fourier transform infrared spectroscopy (FTIR) tests were conducted on powdered samples. The fragment from the compressive test was collected and then vacuum dried for 72 h. Afterward, it was ground immediately. The acquired powders were sieved by using a sieve with a sieve diameter of 45 μm. XRD analysis was conducted by using a Rigaku X-ray diffractometer (D /Max-5A) between 10 and 80° 2θ at a scan speed of 3.0°/min. FTIR analysis was performed by employing a Thermo-Scientific IS10 FTIR workstation and the KBr disc method. A resolution of 2 cm^{-1} with 32 scans was adopted. The thermo-gravimetric analysis (TG) and differential scanning calorimeter (DSC) analysis was conducted by using a Netzsch STA 409 analyzer. The powdered samples were heated up to 1000℃ with a rate of 10℃/min from 30℃. Moreover, scanning electron microscopy (SEM) was performed using FEI Quanta

Table 1
Chemical compositions of PC and CGS (wt.%).

Material	K_2O	Na_2O	SO_3	SiO_2	Fe_2O_3	Al_2O_3	CaO	MgO	Loss
PC	0.3	0.3	/	18.5	3.2	5.8	64.2	/	1.83
CGS	0.44	/	0.28	47.78	2.93	13.63	16.15	2.57	4.73

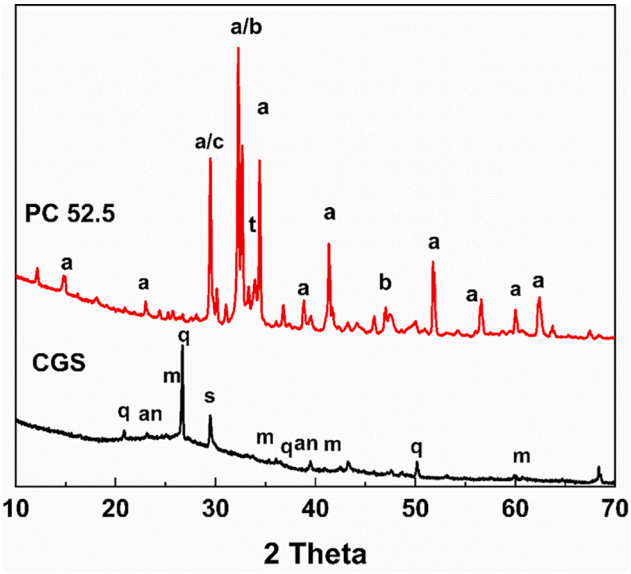

Fig. 2. XRD patterns of PC 52.5 and CGS: a: alite; an: anorthite; b: blite; c: calcite; m: mullite; t: tricalcium aluminate; q: quartz; s: spurrite.

Table 2
Mixture proportions of PC-CGS blends used in this study (wt. %).

No.	CGS	PC	W/B
PC	0	100%	0.4
G1P	10%	90%	
G3P	30%	70%	
G5P	50%	50%	
G7P	70%	30%	

200 scanning electron microscopy at a voltage of 10 keV. The dried samples were coated with gold before the SEM analysis.

3. Results and discussion

3.1. Pozzolanic activity

The Frattini test results for the CGS at 2, 7 and 28 days are shown in Fig. 3. At 2 days, the [Ca] of all groups were above the calcium solubility isotherm, indicating pozzolanic activity did not occur. At the same time, the [CaO] increased when the CGS content increased, showing the stimulation effect on the hydration of PC phases. Moreover, it can be observed that a decrease of [OH^-] when the CGS content increased. This is due to the dilution effect caused by the replacement of PC by CGS. At 7 days, the reduction of [OH^-] and [CaO] showed that CGS with high replacement level (above 50%) have a pozzolanic activity and the test-points are located below the saturation curve. At 28 days, all groups presented proper pozzolanic activity.

3.2. Flowability

The influence of CGS amount on the flowability of the fresh paste is shown in Fig. 4. it can be found that the flowability of the mixture increase from 220 to 243 mm when the CGS content increases from 0% to

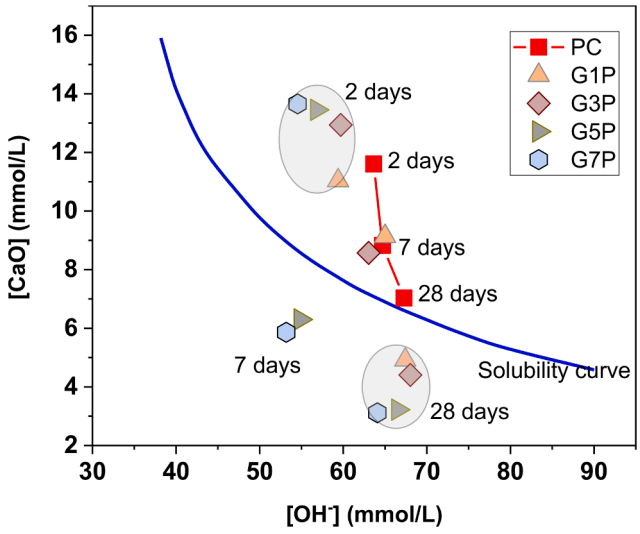

Fig. 3. Frattini test of PC cement with different CGS content at 2, 7 and 28 days.

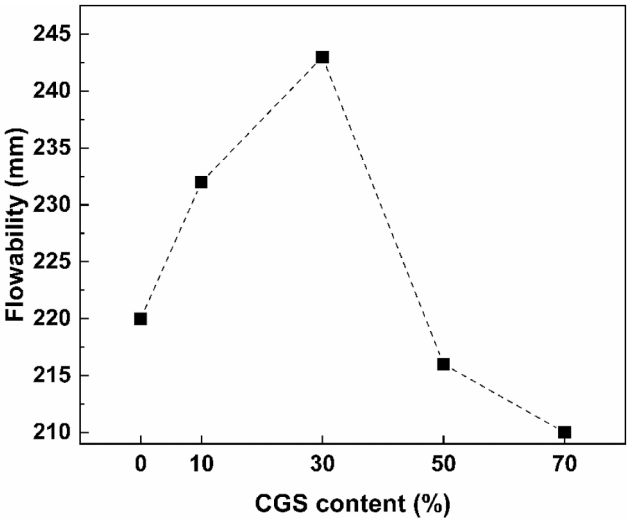

Fig. 4. Flowability of the fresh pastes with different CGS contents.

30%. However, the addition of 70% CGS results in the decrease of the fluidity to 211 mm. The finding in this study is consistent with the previous research [26]. When the CGS content is lower than 30%, the finer CGS particles fill the voids between the PC particles, which would release a certain amount of water, to some extent. On the other hand, the denes surface of the structure of CGS particle plays a positive influence on the flowability. However, the negative impact of the irregular shape of CGS particles and higher specific surface area on the flowability would become more dominant due to increasing the frictional resistance when the CGS content exceeds 30%, thereby considerably decreasing the fluidity.

3.3. Setting times and reaction kinetics

3.3.1. Setting times

The influence of CGS content on the initial and final setting times of the PC paste is depicted in Fig. 5. The inclusion of 10% CGS has little influence on the initial and final setting times, while the initial and final setting times are significantly prolonged when the CGS content exceeds 10%. The initial and final setting times of the paste without CGS are 185 and 276 min, respectively. The incorporation of 10% CGS results in the decrease of the initial and final setting times by 2.7% and 2.6%, respectively, compared with the sample without CGS. However, the initial and final setting times of the sample with 70% CGS increase by 41.8% and 121.8%, respectively, compared with those of the sample without CGS. This is because that when the CGS content exceeds 10%, PC dosage in this system further reduces. As a result, the C_3A content in the system reduces, thus affecting the reaction kinetic of the system [27]. Moreover, it can be observed that the interval between the initial and final setting times increases with the increase of CGS content. This could be because that with the increase of CGS content, less hydration products are formed in the system, which results in the retardation of the final setting time [15,28]. To sum up, it is concluded that the incorporation of CGS can retard the hardening process.

3.3.2. Reaction kinetics

Fig. 6 shows the heat flow of PC pastes with different CGS contents. It can be seen that the shapes of the heat flow curves of the samples with different CGS contents are similar and have four reaction periods corresponding to dissolution, induction, acceleration and deceleration, and stable stages, respectively. The exothermic peak after the wetting and dissolution of binders could be attributed to the precipitation of portlandite and C-S-H [11]. In addition, the induction stage and this exothermic peak occur slightly later when CGS content is higher than 10%. Moreover, with the increase of CGS content, the intensity of this exothermic peak decrease. The paste without CGS shows the highest acceleration peak, whereas the paste with 70% CGS has the weakest one. These findings indicate that the reaction rate of this system is retarded when CGS content exceeds 10% and confirms that the influence of CGS on the reaction rate of PC paste is different from that of other SCMs such as ground granulated blast-furnace slag and limestone [29-31].

The cumulative heat release of the pastes with different CGS contents is depicted in Fig. 7. It can be observed that the first rapid increase corresponds to the wetting and dissolution of starting materials. The next moderate increase is associated with the induction stage and the third increase is assigned to the acceleration stage. The cumulative heat of the sample with 10% CGS is comparable to that of the sample without CGS. However, as the further increase of CGS content, the cumulative heat of the pastes decreases considerably, which indicates that more CGS particles are not involved in the reaction.

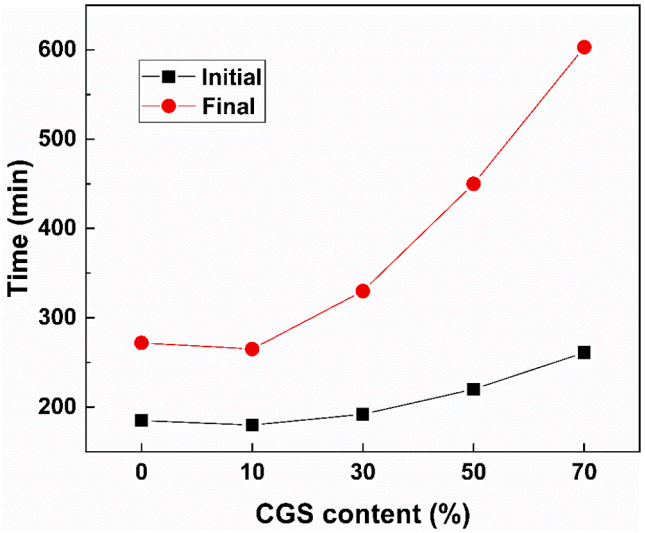

Fig. 5. Effect of CGS content on the initial and final setting times of the paste.

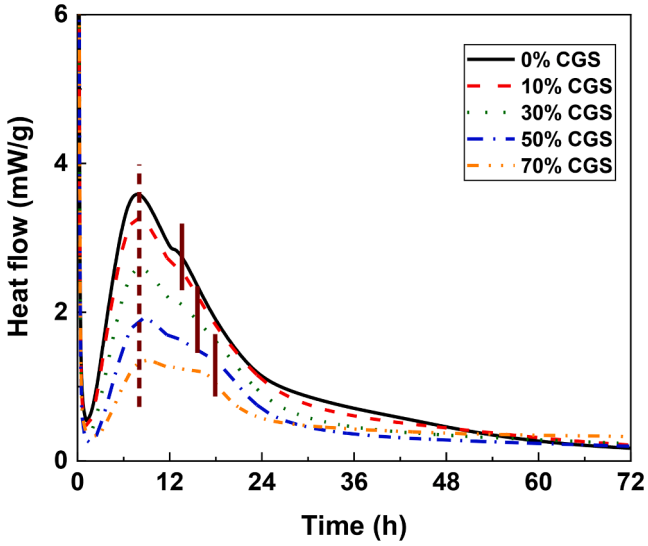

Fig. 6. Heat flow of PC pastes with different CSG contents.

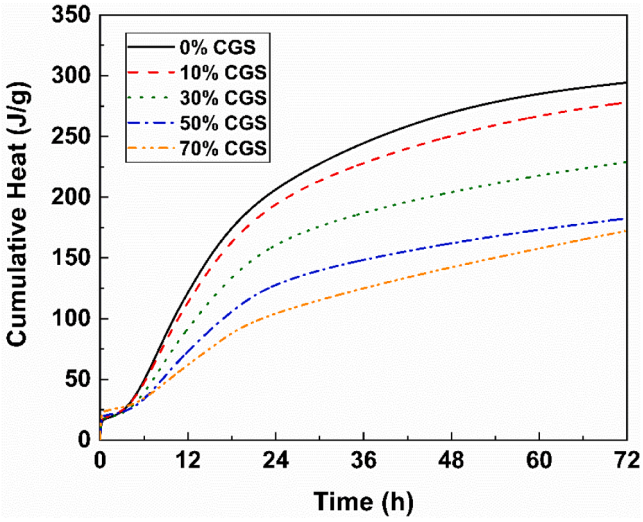

Fig. 7. Cumulative heat of PC pastes with different CGS contents.

3.4. Compressive strength

Fig. 8 shows the effect of CGS content on the compressive strength development of cement paste. As seen from Fig. 8, the addition of 10% CGS powders has a positive effect on the development of the strength of cement paste, especially at the early age. Compared with PC samples without CGS, the strength of 1d, 7d and 28d of G1P increases by 7.1%, 6.9% and 5.4%, respectively. However, further increasing the amount of gasification slag, the compressive strengths of all cement pastes present a decreasing tendency, and the higher the amount of gasification slag, the greater the degree of reduction. Some previous studies [15,20,26] have shown that small amounts of gasification slag admixture can have a beneficial effect on the strength of cement mortars, as their pozzolanic reaction can produce more C-S-H gel. The specific surface area of the gasification slag used in this paper (445 kg/m^3) is larger than that of Portland cement (370 kg/m^3), which could play a filler role in the

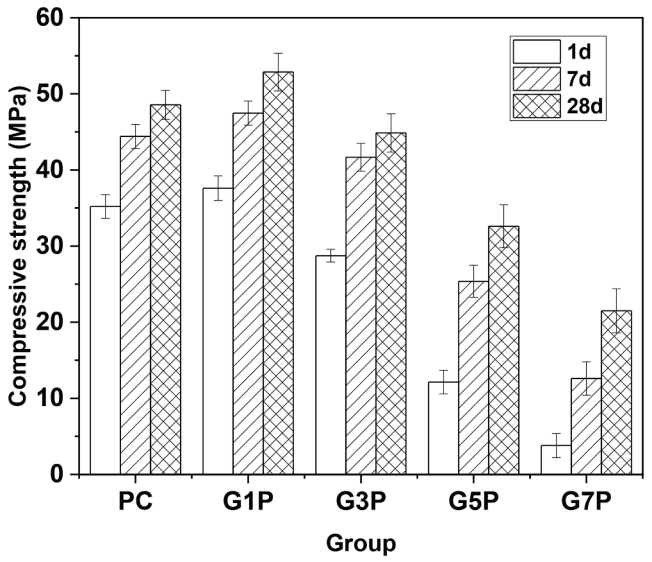

Fig. 8. Effect of gasification slag content on the compressive strength development of the samples.

cement paste, thus reducing the porosity of the system and improving the strength. In addition, the XRD pattern of the gasification slag shows that it contains some amorphous phase, indicating that it has some pozzolanic activity in the alkaline environment of hydration products, which can promote the development of cement hydration. However, due to the limited amount of portlandite in the system, the excessive amount of CGS powder resulted in its inability to react, thus reducing the compressive strength.

3.5. Microstructure

3.5.1. XRd

Fig. 9 shows the XRD patterns of PC paste with different CGS content. The main hydration products of the sample without adding CGS powder after 28 days of curing are portlandite (calcium hydroxide, CH), ettringite (AFt) and calcium silicate hydrate gels (C-S-H). It is noteworthy that all samples contained calcite as a result of carbonation of CH during drying and storage. In contrast, the main hydration product, C-S-H gel, has only very weak peaks in the XRD spectrum due to its amorphous structure, in good agreement with the previous research concentrated on PC paste containing CGS [26]. Therefore, the FTIR analysis on that would be discussed later in this study. As can be seen from Fig. 9, no new hydration products is found in the system after the addition of the CGS powder, except for the characteristic peak of quartz (around 26°), which is introduced from the CGS powder [15]. From each characteristic diffraction peak intensity of the hydration products, compared with the pure cement group (group PC), with adding 10% CGS powder (G1P group), AFt and the corresponding C-S-H gel characteristic peak diffraction intensity increase while CH characteristic peak decrease, indicating that the hydration degree of cement is increased. This demonstrates that the inclusion of 10% CGS promotes the hydration of PC, increasing the degree of hydration and thus the compressive strength of the matrix. According to the previous study by Li et al. [15], the reactive SiO_2 and Al_2O_3 mineral phases in CGS promote the reaction of CGS with PC, facilitating the formation of C-S-H gels and phases with high strength such as calcium alumina and calcite. These hydration products accumulate, then cluster and bond with each other. Eventually, the pore structure of PC is filled with these hydration products, contributing to the improvement of the strength. With the further increase of CGS content, the diffraction intensity of the characteristic peak corresponding to each hydration product decreases significantly, especially in CH. This may be related to the reduction of PC content in the system and the pozzolanic reaction of CGS between active SiO_2 and Al_2O_3 mineral phases in the CGS with CH [15,26].

3.5.2. FTIr

Fig. 10 shows the FTIR spectra of samples with different CGS contents in the range of 400–4000 cm^{-1}. The apparent absorption peaks of H-O-H stretching vibration at around 1650 cm^{-1} for all specimens indicates the presence of chemically bound water in gels [32,33]. The typical O-C-O stretching vibration band at about 1420 cm^{-1} and 875 cm^{-1} [33,34] is found for all specimens indicating that the samples were carbonated during drying and storage, which is consistent with the XRD results. The in-plane bending vibrational band of the Si-O bond occurs around 450 cm^{-1}, which is usually caused by the introduction of SiO_2 from the raw material [33,35,36]. The intensity of this peak increases as the CGS content increases, indicating that the amount of unreacted CGS is increasing. It is worth noting that the band around 700 cm^{-1} is associated with the T-O band in SiO_2 and mullite-like structures, where

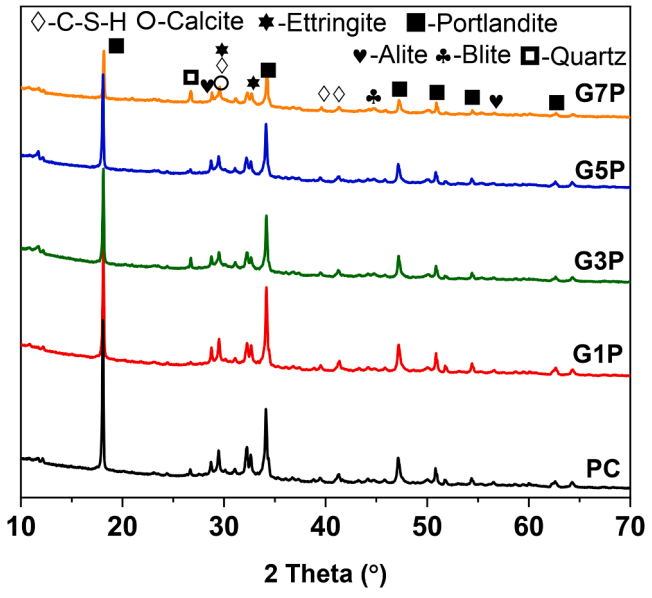

Fig. 9. XRD patterns of PC paste with different CGS contents at 28d.

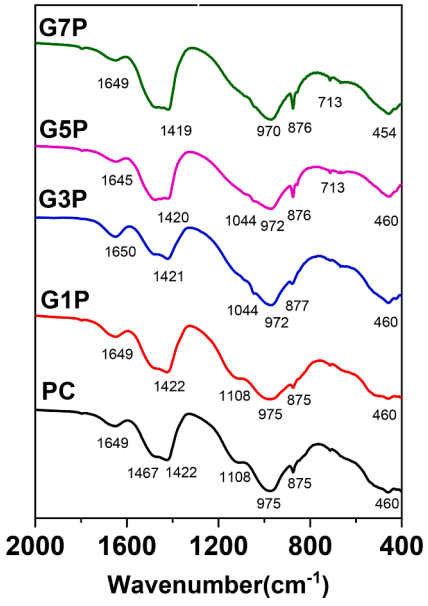

Fig. 10. FTIR spectra of the samples with different CGS contents at 28d.

T stands for silicon or aluminum [37,38]. The position does not change significantly with increasing CGS content, suggesting that CGS does not affect the bending of this bond. At about 970 cm^{-1}, the absorption peak represents the non-uniform stretching vibration of Si-O-T bond, which was well-known as the characteristic peak that results from the C-S-H gel [39]. The absorption peak at 975 cm^{-1} shifted to a lower wavenumber with the increase of CGS content, indicating that the calcium in the cement interacts with the active silica and alumina components in the CGS, causing a reduction in the silica polymerization degree in the C-S-H gels [35,36]. In order to clarify the effect of CGS on the hydration products of C-S-H gels, FTIR spectra in the 800–1300 cm^{-1} range were further analyzed.

According to the previous research [34,40], the four bands at 840 cm^{-1}, 970 cm^{-1}, 1089 cm^{-1} and 1136 cm^{-1} are typical bands of Q_1, Q_2, Q_3 and Q_4 sites assigned to C-S-H gel, respectively. The Q_2 tetrahedron indicates a wide range of C-S-H (Ca/Si ratio≈2:1) and is the most common tetrahedron in well-hydrated cement paste [32,41]. Fig. 11 illustrates the change of main bands in specimens over the range of 800–1300 cm^{-1}, presenting information on four types of vibration of Si-O (Q_1, Q_2, Q_3 and Q_4) in C-S-H gel [39,42]. It can be seen from Fig. 11, that G1P has the highest C-S-H gel content, followed by PC, G3P, G5P and G7P. This indicates that a 10% CGS content favors the formation of the main hydration products of PC paste, which is consistent with the XRD results. The Q_2 band showed the highest peak in G1P samples as the Ca/Si ratio is the highest in C-S-H from the hydration of PC and CGS [41]. On the contrary, the Q_2 site decreased and shifted to a lower wavenumber with the increased CGS content showing the different densities and Ca/Si ratios of C-S-H.

3.5.3. DTG analysis

Fig. 12 shows the DTG results of the samples with different CGS contents at 28d. There are three distinct characteristic peaks observed in Fig. 12. The first one is at 30–170 °C and is due to the dehydration of AFm (70 °C), C-S-H (100 °C) and calcium alumina (AFt phase) (150 °C) [43]. The second one is at 400–470 °C and is attributed to calcium hydroxide. Finally, at 610–720 °C, this peak is attributed to the decomposition of calcium carbonate due to the carbonation of calcium hydroxide during the process. Usually, the first and second peaks reflect the amount of hydration products. The compressive strength of the sample is strongly dependent on the areas of these peaks [44]. As can be seen in Fig. 12, the sum of the mass loss of the first and second peaks is 14%, 14.5%, 10.8%, 10.4% and 6.9%, respectively, which indicates that G1C has a higher extent of hydration at 28d. Furthermore, G1P has the highest heat loss mass of 10.3% in the first endothermic peak, while PC has the highest heat loss mass of 5.4% in the second peak, indicating that the 10% CGS admixture effectively results in the promotion of the hydration and the occurrence of the pozzolanic effect that consumes the amount of CH and promotes the production of C-S-H and AFt as well, thus causing an increase in the compressive strength. Moreover, it can be found the incorporations of 10%-30% CGS results in the increase of the area of the characteristic peak at 610–720 °C, implying the increase of the amount of calcium carbonate. It could be attributed to the carbonation of calcium hydroxide and C-S-H gel during the curing and storage process. It has been confirmed earlier that adding CGS supports pozzolanic reaction and promotes the formation of C-S-H gel. Therefore, it is possible that more C-S-H gel could be carbonated, which finally results in the increase of the amount of calcium carbonate. To sum up, when the content of CGS is less than 30%, CGS exhibits a positive influence. However, a further increase in CGS admixture results in a significant decrease in the formation of hydration products, indicating that excessive CGS particles did not participate in the reaction. This is consistent with the results of XRD and FTIR analyses.

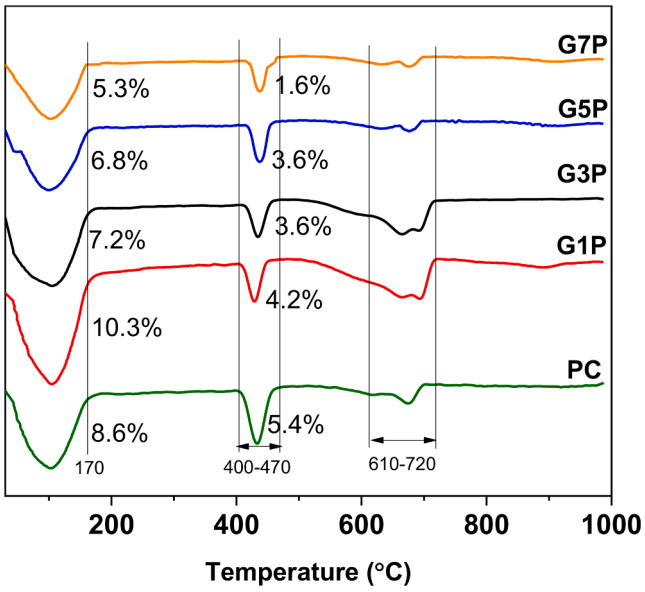

Fig. 12. DTG results of PC samples with different CGS contents at 28d.

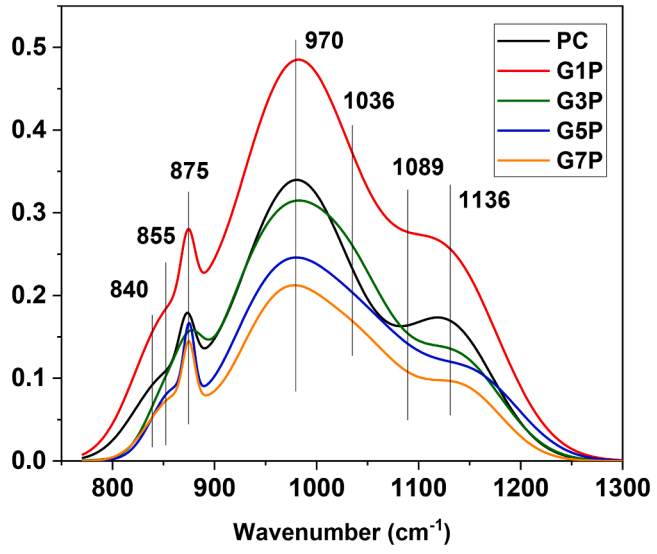

Fig. 11. Change of the Si-O bands of PC with different CGS content at 28 d.

3.5.4. SEM analysis

Fig. 13 shows SEM images of samples with different CGS content at 28 d. Fig. 13 (a) is the SEM image of the sample without adding CGS powder, in which needle-stick ettringite, flake calcium hydroxide [45] and massive C-S-H gel can be clearly observed [46]. Fig. 13 (b) shows the SEM image of cement paste with 10% CGS powder. Compared with the sample without CGS powder (Fig. 13 (a)), unhydrated CGS particles are found in the system, and it can be seen that most the CGS powder exists in the cement matrix in a state of agglomeration. Some fine crystals can also be seen in Fig. 13 (b) as well, which could be considered as the hydration product particles formed by the pozzolanic reaction of finer CGS particles. This indicates the pozzolanic effect of CGS powders in PC. On the other hand, fine mineral admixtures can play a role as nucleation in PC [47,48]. Consequently, a certain amount of reactive mineral admixtures in cement contributes to the formation of reaction products. On the other hand, with the increasing of curing age, C-S-H gel and CH gradually precipitate and cluster on the surface of mineral admixtures. Therefore, it can be inferred that CGS powder has a nucleate effect, similar to other mineral admixtures. In other words, it can be explained that, compared with the sample without CGS (Fig. 13 (a)), the peak intensity of C-S-H gel in the FTIR spectrum and the compressive strength of the sample with 10% CGS powder are significantly increased.

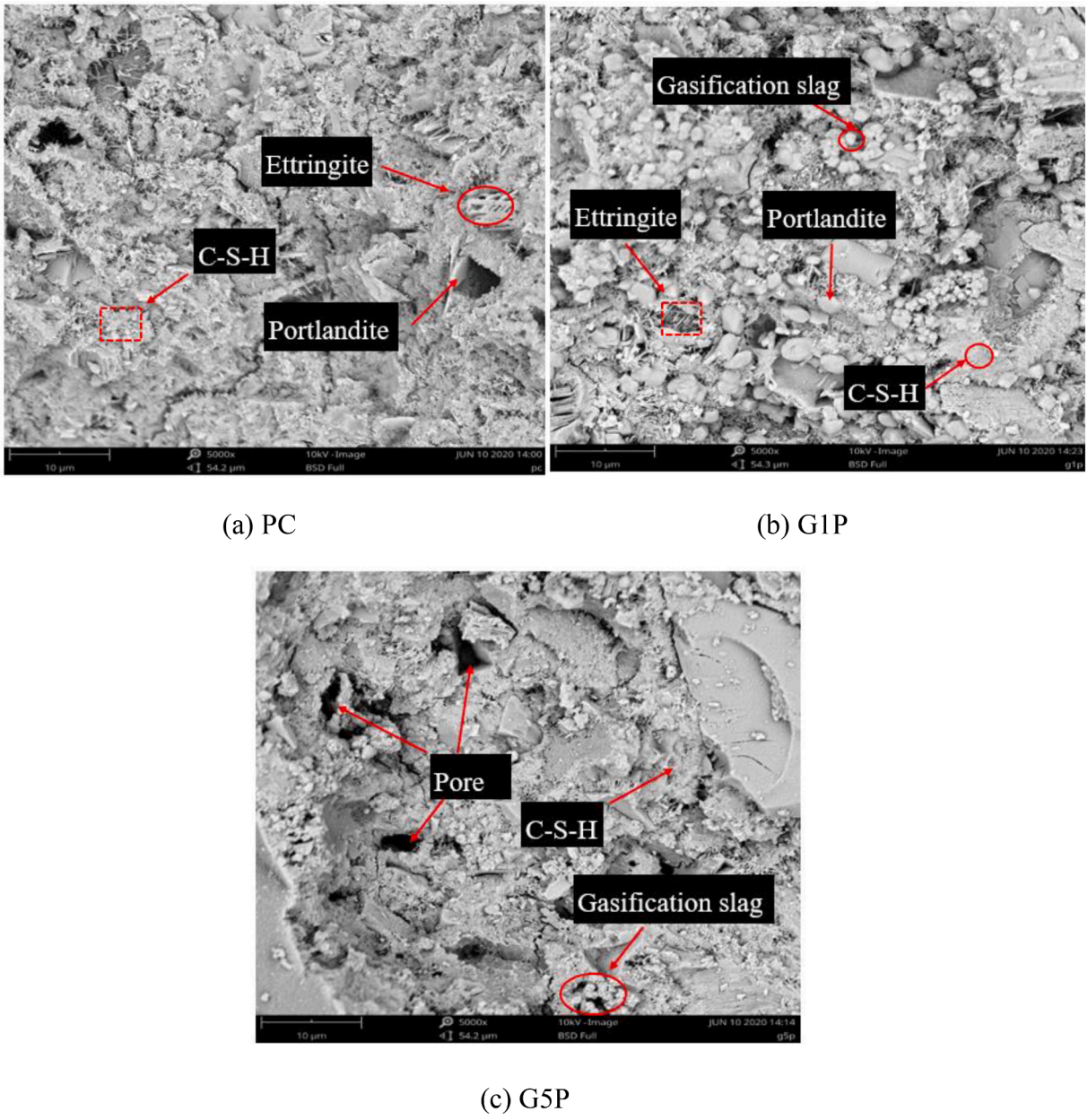

(a) PC (b) G1P

(c) G5P

Fig. 13. SEM images of PC samples with different CGS content at 28d.

Fig. 13 (c) is the SEM image of cementite with 50% CGS powder. It can be seen that compared with the sample containing 10% CGS powder, more agglomerated CGS particles are observed, and the needle-stick ettringite particles almost disappear. The porosity of reaction products increases and the looseness of the microstructure increases, thus leading to a reduction in the compressive strength.

4. Conclusions

CGS was used as reactive mineral additive in PC blends. The influence of CGS content on the setting times, reaction kinetics, compressive strength and microstructure was evaluated. The following conclusion can be drawn based on the results:

(1) Frattini test results showed that no pozzolanic activity occurred in CGS on day 2, regardless of the dosage. On day 7, the paste with high CGS content (>50%) showed pozzolanic activity, while on day 28, all dosage groups presented proper pozzolanic activity.
(2) The initial and final setting times were influenced by the CGS content. A higher CGS content (>10%) resulted in a significantly decreased setting time. The addition of 10% CGS slightly accelerated the induction and acceleration/deceleration stage. However, with the further increase of CGS dosage, the retardation of the reaction process was found. Also, the inclusion of CGS led to the reduction of the reaction intensity and cumulative heat release.
(3) Compared with PC samples, the strength of 1d, 7d and 28d of G1P increased by 7.1%, 6.9% and 5.4%, respectively. The 10% admixture of CGS significantly increased the early strength of the cement paste. However, the compressive strength of the samples decreased when the CGS content exceeded 10%.
(4) The microstructure analysis performed by XRD, FTIR, TG and SEM showed that the incorporation of 10% CGS powder could effectively improve the microstructure and resultant compressive

strength. Proper CGS content can play a nucleation and pozzolanic effect, which is conducive to accelerating the reaction process, facilitating the formation of the hydration products, and refining the microstructure. As a result, the compressive strength was improved.

CRediT authorship contribution statement

Bo Fu: Conceptualization, Methodology, Writing – original draft, Writing – review & editing, Funding acquisition. **Zhenyun Cheng:** Software, Writing – original draft. **Dezhi Wang:** Writing – review & editing. **Ning Li:** Conceptualization, Supervision, Writing – review & editing.

Declaration of Competing Interest

The authors declare that they have no known competing financial interests or personal relationships that could have appeared to influence the work reported in this paper.

Acknowledgement

We gratefully acknowledge the National Natural Science Foundation of China (51668001 and 51968060), Key research and development program of Ningxia (2020BDE03009), Natural Science Foundation of Ningxia (2020AAC03195 and 2021AAC03187). The participation of Ning Li was supported by the Postdoctoral Science Foundation of China (2020M680113).

References

[1] L. Szabó I. Hidalgo J.C. Císcar A. Soria P. Russ Energy consumption and CO2 emissions from the world cement industry 2003.
[2] K.L. Scrivener, V.M. John, E.M. Gartner, Eco-efficient cements: Potential economically viable solutions for a low-CO2 cement-based materials industry, Cement Concr. Res. 114 (2018) 2–26.
[3] D.B. Müller, G. Liu, A.N. Løvik, R. Modaresi, S. Pauliuk, F.S. Steinhoff, H. Brattebø, Carbon Emissions of Infrastructure Development, Environ. Sci. Technol. 47 (20) (2013) 11739–11746.
[4] D.L. Summerbell, C.Y. Barlow, J.M. Cullen, Potential reduction of carbon emissions by performance improvement: A cement industry case study, J. Clean. Prod. 135 (2016) 1327–1339.
[5] Y. Izumi, A. Iizuka, H.-J. Ho, Calculation of greenhouse gas emissions for a carbon recycling system using mineral carbon capture and utilization technology in the cement industry, J. Clean. Prod. 312 (2021), 127618.
[6] M. Schneider, M. Romer, M. Tschudin, H. Bolio, Sustainable cement production—present and future, Cement Concr. Res. 41 (7) (2011) 642–650.
[7] R.I. Iacobescu, G.N. Angelopoulos, P.T. Jones, B. Blanpain, Y. Pontikes, Ladle metallurgy stainless steel slag as a raw material in Ordinary Portland Cement production: a possibility for industrial symbiosis, J. Clean. Prod. 112 (2016) 872–881.
[8] B. Lothenbach, K. Scrivener, R.D. Hooton, Supplementary cementitious materials, Cement Concr. Res. 41 (12) (2011) 1244–1256.
[9] J. Liu, B. Yu, Q. Wang, Application of steel slag in cement treated aggregate base course, J. Clean. Prod. 269 (2020), 121733.
[10] O. Najm, H. El-Hassan, A. El-Dieb, Ladle slag characteristics and use in mortar and concrete: a comprehensive review, J. Clean. Prod. 288 (2021) 125584, https://doi.org/10.1016/j.jclepro.2020.125584.
[11] S. Zhuang, Q. Wang, Inhibition mechanisms of steel slag on the early-age hydration of cement, Cement Concr. Res. 140 (2021), 106283.
[12] M. Li, J. Zhang, A. Li, N. Zhou, Reutilisation of coal gangue and fly ash as underground backfill materials for surface subsidence control, J. Clean. Prod. 254 (2020), 120113.
[13] J. Zhang, S. Zhang, B.o. Liu, Degradation technologies and mechanisms of dioxins in municipal solid waste incineration fly ash: A review, J. Clean. Prod. 250 (2020) 119507, https://doi.org/10.1016/j.jclepro.2019.119507.
[14] S.N. Minnu, A. Bahurudeen, G. Athira, Comparison of sugarcane bagasse ash with fly ash and slag: An approach towards industrial acceptance of sugar industry waste in cleaner production of cement, J. Clean. Prod. 285 (2021), 124836.
[15] Z. Li, Y. Zhang, H. Zhao, H. Chen, R. He, Structure characteristics and composition of hydration products of coal gasification slag mixed cement and lime, Constr. Build. Mater. 213 (2019) 265–274.
[16] X. Liu, Z. Jin, Y. Jing, P. Fan, Z. Qi, W. Bao, J. Wang, X. Yan, P. Lv, L. Dong, Review of the characteristics and graded utilisation of coal gasification slag, Chin. J. Chem. Eng. 35 (2021) 92–106.
[17] T. Wu, M. Gong, E.d. Lester, F. Wang, Z. Zhou, Z. Yu, Characterisation of residual carbon from entrained-bed coal water slurry gasifiers, Fuel 86 (7-8) (2007) 972–982.
[18] I. Yoshitaka, Utilization of coal gasification slag collected from IGCC as fine aggregate for concrete, Chigaski-City, Kanagawa, Chigasaki, 2012, pp. 25–27.
[19] M. Aineto, A. Acosta, J.M. Rincón, M. Romero, Production of lightweight aggregates from coal gasification fly ash and slag, World of Coal Ash (WOCA) (2005) 11-15.
[20] R. Pomykała, The mechanical properties of coal gasification slag as a component of concrete and binding mixtures, Polish J. Environ. Stud. 23 (4) (2014) 1403–1485.
[21] ASTM C305, Standard practice for mechanical mixing of hydraulic cement pastes and mortars of plastic consistency, 2006.
[22] EN 196, Cements Test Methods: Pozzolanic test for Pozzolanic cements (in Spanish), 2005.
[23] ASTM C 230, Standard specification for sample and testing fly ash or natural pozzolan for use as a mineral admixture in Portland cement, 1997.
[24] GBT 1346, Test methods for water requirement of normal consistency, setting time and soundness of the Portland cement (in Chinese), 2011.
[25] ASTM C191, Standard test methods for time of setting of hydraulic cement by Vicat needle, 2008.
[26] F. Luo, Y. Jiang, C. Wei, Potential of decarbonized coal gasification residues as the mineral admixture of cement-based material, Constr. Build. Mater. 269 (2021), 121259.
[27] P. Shafigh, S. Yousuf, Z. Ibrahim, B. Alsubari, I. Asadi, Influence of fly ash and GGBFS on the pH value of cement mortar in different curing conditions, Adv. Concr. Construct. 11권(5호) (2021) 419-428.
[28] C.O. Nwankwo, G.O. Bamigboye, I.E.E. Davies, T.A. Michaels, High volume Portland cement replacement: A review, Constr. Build. Mater. 260 (2020) 120445, https://doi.org/10.1016/j.conbuildmat.2020.120445.
[29] C. Shi, D. Wang, L. Wu, Z. Wu, The hydration and microstructure of ultra high-strength concrete with cement–silica fume–slag binder, Cem. Concr. Compos. 61 (2015) 44–52.
[30] D. Wang, C. Shi, N. Farzadnia, Z. Shi, H. Jia, Z. Ou, A review on use of limestone powder in cement-based materials: Mechanism, hydration and microstructures, Constr. Build. Mater. 181 (2018) 659–672.
[31] S. Drissi, C. Shi, N. Li, Y. Liu, J. Liu, P. He, Relationship between the composition and hydration-microstructure-mechanical properties of cement-metakaolin-limestone ternary system, Constr. Build. Mater. 302 (2021), 124175.
[32] P. Yu, R.J. Kirkpatrick, B. Poe, P.F. McMillan, X. Cong, Structure of Calcium Silicate Hydrate (C-S-H): Near-, Mid-, and Far-Infrared Spectroscopy, J. Am. Ceram. Soc. 82 (3) (1999) 742–748.
[33] A. Fernández-Jiménez, A. Palomo, Composition and microstructure of alkali activated fly ash binder: Effect of the activator, Cement Concr. Res. 35 (10) (2005) 1984–1992.
[34] N. Li, N. Farzadnia, C. Shi, Microstructural changes in alkali-activated slag mortars induced by accelerated carbonation, Cement Concr. Res. 100 (2017) 214–226.
[35] S.A. Bernal, E.D. Rodríguez, R. Mejia de Gutiérrez, J.L. Provis, S. Delvasto, Activation of metakaolin/slag blends using alkaline solutions based on chemically modified silica fume and rice husk ash, Waste Biomass Valorization 3 (1) (2012) 99–108.
[36] F. Puertas, S. Martínez-Ramírez, S. Alonso, T. Vázquez, Alkali-activated fly ash/slag cements: Strength behaviour and hydration products, Cement Concr. Res. 30 (10) (2000) 1625–1632.
[37] D. Voll, C. Lengauer, A. Beran, H. Schneider, Infrared band assignment and structural refinement of Al-Si, Al-Ge, and Ga-Ge mullites, Eur. J. Mineral. 13 (3) (2001) 591–604.
[38] N. Li, C. Shi, Q. Wang, Z. Zhang, Z. Ou, Composition design and performance of alkali-activated cements, Mater. Struct. 50 (3) (2017) 178.
[39] R. Ylmén, L. Wadsö, I. Panas, Insights into early hydration of Portland limestone cement from infrared spectroscopy and isothermal calorimetry, Cement Concr. Res. 40 (10) (2010) 1541–1546.
[40] X. Pan, Z. Shi, C. Shi, X. Hu, L. Wu, Interactions between inorganic surface treatment agents and matrix of Portland cement-based materials, Constr. Build. Mater. 113 (2016) 721–731.
[41] I. García-Lodeiro, A. Fernández-Jiménez, M.T. Blanco, A. Palomo, FTIR study of the sol–gel synthesis of cementitious gels: C-S–H and N–A–S–H, J. Sol-Gel Sci. Technol. 45 (1) (2008) 63–72.
[42] Y. Wu, G. Jiang, J. You, H. Chen, Progress of research on micro structure of amorphous silicate, J. Chin. Ceram. Soc. 32 (2004) 57–62.
[43] B. Lothenbach, F. Winnefeld, C. Alder, E. Wieland, P. Lunk, Effect of temperature on the pore solution, microstructure and hydration products of Portland cement pastes, Cement Concr. Res. 37 (4) (2007) 483–491.
[44] N. Billong, J. Oti, J. Kinuthia, Using silica fume based activator in sustainable geopolymer binder for building application, Constr. Build. Mater. 275 (2021), 122177.
[45] L. Zhang, K. Yamauchi, Z. Li, X. Zhang, H. Ma, S. Ge, Novel understanding of calcium silicate hydrate from dilute hydration, Cement Concr. Res. 99 (2017) 95–105.
[46] I.G. Richardson, The nature of C-S-H in hardened cements, Cement Concr. Res. 29 (8) (1999) 1131–1147.
[47] D.P. Bentz, Modeling the influence of limestone filler on cement hydration using CEMHYD3D, Cem. Concr. Compos. 28 (2) (2006) 124–129.
[48] X. Gao, Q.L. Yu, H.J.H. Brouwers, Characterization of alkali activated slag–fly ash blends containing nano-silica, Constr. Build. Mater. 98 (2015) 397–406.